中國機械工程學刊第四十三卷第一期第 47~56 頁(民國一百一十一年)
Journal of the Chinese Society of Mechanical Engineers, Vol.43, No.1, pp 47~56 (2022)

Numerical Analysis on the Ethanol Steam Reforming in a Tubular Fixed-Bed Reactor

Wen-Jenn Sheu*, Chu-Yu Huang* and Yen-Cho Chen**

Keywords : Hydrogen production, ethanol steam reforming, tubular fixed-bed reactor.

ABSTRACT

The ethanol steam reforming for hydrogen production in a tubular fixed-bed reactor is investigated numerically. The effects from the wall temperature (T_w), the gas hourly space velocity (GHSV), and the inlet molar ratio of steam to ethanol (ψ) are analyzed. For GHSV = 2000 h^{-1}, the results show that for a higher T_w of 873 K and ψ =10, the methane molar concentration in the vicinity of inlet region is greater than that at outlet where an equilibrium state approaches. However, this phenomenon disappears for T_w = 673 K. The results reveal that a high ratio (78.2%) of produced hydrogen for ψ = 3 comes from the steam at T_w = 673 K, and the ratio of H_2 coming from the steam is remarkably decreased with increasing T_w, and more than 50% of hydrogen comes from steam for T_w < 852 K. But for ψ = 10, the ratio of H_2 coming from the steam is always slightly lower than that of H_2 coming from the ethanol. Based on the parameters in this work, at least 45% of produced hydrogen comes from the steam.

INTRODUCTION

Hydrogen is clean energy carrier and used as the fuel for fuel cell (Wang et al., 2020). Most of the world's hydrogen is produced via fossil fuels–a non-renewable energy source (Nikolaidis et al., 2017), since it is the most economically competitive method for hydrogen production. However, the huge amount of carbon dioxide emission is accompanied with this conventional hydrogen production process. Since CO_2 is the major greenhouse gas, there is a growing effect in the search the alternatives to produce renewable hydrogen. Ni et al. (2007) indicated that ethanol was very attractive among the non-fossil feedstock because of its relatively high hydrogen content, availability, non-toxicity, and storage and handling safety. Ethanol can be produced renewably from biomass sources.

There are three types of reforming process to produce hydrogen from hydrocarbon fuel: steam reforming, partial oxidation, and autothermal reforming. An overview of hydrogen production technologies was given by Holladay et al. (2009). Steam reforming is widely used for producing hydrogen, since it has a lower operating temperature and higher hydrogen yield (Chang, et al., 2019; Chen and Lin, 2010; Perng, et al., 2019; Huang et al., 2020). The produced hydrogen by steam reforming method comes from both fuel and steam, while it only comes from fuel by partial oxidation method.

The CO concentration after steam reforming is much larger than the tolerance value (< 10 ppm) when the reformed syngas is supplied as fuel for the low temperature type of PEM fuel cell. The water-gas shift reaction is often used to reduce the CO concentration by converting CO and steam to CO_2 and hydrogen (Chen et al., 2008; Chen and Chen, 2020). A membrane reactors integrated with water gas shift reaction, where only the hydrogen can penetrate the palladium membrane, is used to reduce the CO concentration of the reformed syngas to very low value (Chen and Lu, 2012; Lin et al., 2020).

A review article by Ni et al. (2007) indicated that Rh and Ni were the most commonly used catalysts for ethanol steam reforming, and MgO, ZnO, CeO_2, and La_2O_3 were suitable supports for Rh and Ni, which favor ethanol dehydrogenation but inhibit dehydration. Steam reforming of ethanol was investigated over MgO supported Ni and Co catalysts by Freni et al. (2003). Their results showed that Ni/MgO catalysts exhibit higher activity and selectivity to H_2 than Co/MgO catalysts because of the lower tendency of Ni to oxidize during reaction and to promote CO methanation and ethanol decomposition reactions.

The ethanol steam reforming on $Ni/\gamma Al_2O_3$

Paper Received August, 2020. Revised September, 2020. Accepted October, 2020. Author for Correspondence: Yen-Cho Chen. E-mail: ycchen@nuu.edu.tw

Department of Power Mechanical Engineering, National Tsing Hua University, Hsinchu, 30013, Taiwan, R.O.C.

**Department of Energy Engineering, National United University, Miaoli, 36063, Taiwan, R.O.C.*

catalyst between 573 and 773 K was studied and an overall reaction scheme as a function of temperature was proposed by Comas et al. (2004). They found that higher steam/ethanol ratio (6:1) and higher temperature (773 K) promote hydrogen production (91% selectivity). The catalytic activities of three nickel catalysts Ni/Y_2O_3, Ni/La_2O_3, and Ni/Al_2O_3 for the ethanol steam reforming were investigated by Sun et al. (2005). It was found that the ethanol conversions for Ni/Y_2O_3 and Ni/La_2O_3 at 320 °C were 93.1% and 99.5% and the values of hydrogen selectivity were 53.2% and 48.5%, respectively. The three catalysts all had long-term stability.

Kinetic study of ethanol steam reforming over a commercial $Ni/MgO/Al_2O_3$ catalyst in a fixed-bed reactor was conducted by Mathure et al. (2007). Maximum conversion (> 95%) was obtained at 873 K, with a molar ratio of steam to ethanol of 12:1 at atmospheric pressure. Akande et al. (2006) performed a kinetic modeling for the crude ethanol reforming over a 15% Ni/Al_2O_3 catalyst in a packed bed tubular reactor at 1atm between 593–793 K. A kinetic model based on the dissociation of adsorbed crude ethanol as the rate-determining step was developed for this catalytic process.

Steam reforming of bio-ethanol over Ni/CeO_2–ZrO_2 and Rh–Ni/CeO_2–ZrO_2 catalysts was studied by Mondal et al. (2015). Their results revealed that addition of ZrO_2 improved catalytic activity and Rh promoted catalyst exhibited better catalytic activity than 30%Ni/CeO_2–ZrO_2 catalyst. Complete ethanol conversion was achieved at 600 °C with a maximum hydrogen yield of 4.6 mol/mol A review of catalysts for the ethanol steam reforming was given by Contreras et al. (2014).

Wu et al. (2014) carried out the kinetic studies over a nickel-based catalyst for ethanol steam reforming. A simplified Langmuir–Hinshelwood–Hougen–Watson (LHHW) kinetic model was proposed. The proposed kinetic model works well over a wide temperature range (200–600°C). Mechanistic kinetic models based on LHHW and Eley–Rideal approaches for the crude ethanol reforming over a Ni-based catalyst at 673–863 K in a packed bed tubular microreactor were studied by Akpan et al. (2007). The predicted ethanol conversion was in good agreement with the experimental data. The concentration and temperature profiles in the radial direction indicated that the assumption of plug flow was justified. But the axial dispersion term cannot be neglected.

A kinetic study of steam reforming of ethanol using a nickel based catalyst at 873–923 K was performed by Llera et al. (2012). Their results showed that more than 5 moles of hydrogen per mole of ethanol at 923 K were obtained and the surface reactions were the rate-determining steps. A 2-D CFD model on the ethanol steam reforming within a catalytic membrane reactor was developed by Ma et al. (2018). A comprehensive heat and mass transfer study was carried out. Their results showed that a “cold spot” was seen at the reactor entrance area and the reverse methane steam reforming (methanation) was observed, caused by the low temperature in the “cold spot”.

From the above literature review, the research works on ethanol steam reforming in the past were mainly focused on the performance of different catalysts and catalyst supports, and reaction kinetic modeling. The experimental work and numerical modeling in the fixed-bed reactor are limited especially for results of the variation of distributions of species concentration with GHSV, T_w and inlet molar ratio of steam to ethanol. Therefore, the numerical analysis of ethanol steam reforming in a tubular fixed-bed reactor is studied in this work. The produced hydrogen comes from both fuel and steam in ethanol steam reforming. As a result, it is interest to investigate the ratios of hydrogen gas generated from fuel and steam respectively.

MATHEMATICAL FORMULATION

A schematic of ethanol steam reforming in a tubular fixed-bed reactor with constant wall temperature, T_w, is shown in Fig. 1. The reactor has a radius of R and a length of L. The catalyst bed is filled uniformly with Ni/Al_2O_3 grains. The porosity of the catalyst bed is 0.649 (Cunha et al., 2012). A C_2H_5OH/H_2O mixture with the steam/ethanol molar ratio of ψ and temperature of T_{in} is supplied from the inlet into the catalyst bed.

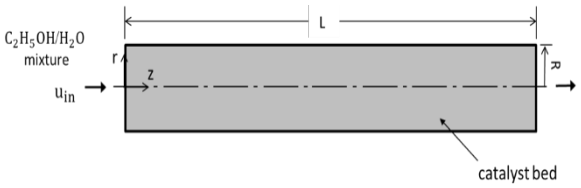

Fig. 1 A schematic of ethanol steam reforming in a tubular fixed-bed reactor.

Governing equations

The following assumptions are made to simplify the mathematical model:

1. Flows are steady, laminar and axisymmetric.
2. All gas species and mixtures are treated as ideal compressible gases.
3. The ethanol-steam mixture at the inlet is completely vaporized.
4. The catalyst pellet is spherical with diameter d_p and the packed bed formed by the catalyst pellet

is treated as a homogeneous porous medium with porosity ε and permeability *K*.

(5) The catalyst bed is in local thermal equilibrium with the surrounding gas mixture.

(6) No sintering and carbon deposition occur in the catalyst during the reaction.

Based on the above assumptions, the governing equations for mass conservation, momentum, energy and species transport in the reactor are written as,

$$\nabla \cdot \left(\varepsilon \rho_g \vec{V}\right) = 0 \tag{1}$$

$$\frac{1}{\varepsilon^2}\nabla \cdot (\rho \vec{V}\vec{V}) = \nabla \cdot \left[-p\vec{I} + \frac{\mu_m}{\varepsilon}\left(\nabla \vec{V} + (\nabla \vec{V})^T - \frac{2\mu_m}{3\varepsilon}\vec{I}\nabla \cdot \vec{V}\right)\right] + S_u \tag{2}$$

$$\nabla \cdot (\varepsilon \rho C_p \vec{V} T) = \nabla \cdot (\lambda_e \nabla T) + q_c \tag{3}$$

$$\nabla \cdot \left\{ \rho \vec{V} m_i - \rho m_i \sum_{j=1}^{N} \left[D_{ij}\left(\nabla y_i - (y_i - m_i)\frac{\nabla p}{p}\right) - D_i^T \frac{\nabla p}{p}\right]\right\} = r_i \tag{4}$$

Eq. (2) is known as the Darcy-Brinkman equation in which $\vec{V}$ is the flow velocity vector, *P* is the pressure, μ_m is the gas mixture viscosity and ρ is the mass-weighted density of gas mixture defined as,

$$\rho = \frac{p}{R_g T}\sum_{j=1}^{N} y_i M_i \tag{5}$$

where *N* is the number of gas species, y_i and M_i are the species molar fraction and molecular weight, respectively. The S_U in Eq. (2) is expressed by as,

$$S_u = -\frac{\mu_m}{K}\vec{V} + \frac{\rho C_F}{\sqrt{K}}\left|\vec{V}\right|\vec{V} \tag{6}$$

The permeability *K* and Forchheimer drag coefficient C_F for a packed bed with spherical particles can be written as,

$$K = d_p^2 \varepsilon^3 / [150(1-\varepsilon)^2], \quad C_f = 1.75/(\sqrt{150}\varepsilon^{1.5}) \tag{7}$$

T in Eq. (3) is the temperature, and q_c is the source/sink due to chemical reaction. The specific heat, C_p, and the effective thermal conductivity, λ_e, in Eq. (3) are given by,

$$C_p = \sum_{j=1}^{N} y_i C_{p,i}, \quad \lambda_e = \varepsilon \lambda_m + (1-\varepsilon)\lambda_s \tag{8}$$

where $C_{p,i}$ is the specific heat of species *i*. λ_s is the thermal conductivity of the catalyst particle and λ_m is the thermal conductivity of gas mixture.

Eq. (4) is known as the Maxwell-Stefan species transport equation. The m_i, r_i, D_{ij} and D_i^T are the mass fraction, production rate due to chemical reactions, binary gas diffusivity and thermal diffusion coefficient of the ith species, respectively. In these equations the gas mixture transport properties (μ_m, λ_m, D_{ij} and D_i^T) can be evaluated based on the Chapman-Enskog theory (Bird et al., 2002).

Chemical Reaction Model

By using Ni/Al_2O_3 as the catalyst, the overall ethanol steam reforming ($C_2H_5OH + 3H_2O \rightarrow 6H_2 + 2CO_2$) is composed of three overall reactions as follows (Sun et al., 2005),

ethanol decomposition:

$$C_2H_5OH \rightarrow CH_4 + CO + H_2 \qquad \Delta H = 49 \text{ kJ/mol} \tag{9}$$

methane steam reforming:

$$CH_4 + H_2O \rightleftharpoons CO + 3H_2 \qquad \Delta H = 205.9 \text{ kJ/mol} \tag{10}$$

water-gas shift reaction:

$$CO + H_2O \rightleftharpoons CO_2 + H_2 \qquad \Delta H = -41 \text{ kJ/mol} \tag{11}$$

The kinetics used in our model can be expressed as, Ethanol decomposition (Ma et al., 2018):

$$r_1 = k_1 P y_{C_2H_5OH} \tag{12}$$

Methane steam reforming (Xu et al., 1989):

$$r_2 = \frac{k_2 y_{H_2}^{2.5}(y_{CH_4} y_{H_2O} - y_{CO} y_{H_2}^3 P^2 / K_3)}{(DEN^2 \sqrt{P})} \tag{13}$$

Water gas shift (Xu et al., 1989):

$$r_3 = \frac{k_3 P(y_{CO} y_{H_2O} - y_{CO_2} y_{H_2} / K_2)}{(y_{H_2} DEN^2)} \tag{14}$$

$$DEN = 1 + P\left(K_{CO} y_{CO} + K_h y_{H_2} + K_M y_{CH_4}\right) + K_W y_{H_2O}/y_{H_2} \tag{15}$$

The unit of r_1, r_2, or r_3 is mol/(g_{cat} · s). The reaction rate constants $k_1, k_2,$ and k_3 are expressed as,

$$k_1 = 4.55 \times 10^{-5}/T \cdot exp(-2030/T) \tag{16a}$$

$$k_2 = 3.711 \times 10^{14} \cdot exp(-28879/T) \tag{16b}$$

$$k_3 = 5.43 \times 10^{-3} \cdot exp(-8074.33/T) \tag{16c}$$

The reaction equilibrium constant s K_2 and K_3 are expressed as

$$K_2 = 10^{10} \cdot exp(-26830/T + 30.114) \tag{17a}$$

$$K_3 = exp(4400/T - 4.036) \tag{17b}$$

In Eq. (15) K_{CO}, K_h, K_M and K_W are expressed as

$$K_{co} = 8.23 \times 10^{-10} \cdot exp(8497.71/T) \qquad (18a)$$

$$K_m = 6.64 \times 10^{-9} \cdot exp(4604.28/T) \qquad (18b)$$

$$K_h = 6.12 \times 10^{-14} \cdot exp(9971.13/T) \qquad (18c)$$

$$K_w = 1.77 \times 10^{5} \cdot exp(-10666.35/T) \qquad (18d)$$

The production rate r_i in Eq. (4) and q_c in Eq. (3) are given by,

$$r_{CH_5OH} = -r_1 \times \frac{W_{cat}}{V_{cat}} \times M_{CH_5OH} \qquad (19a)$$

$$r_{CH_4} = (r_1 - r_2) \times \frac{W_{cat}}{V_{cat}} \times M_{CH_4} \qquad (19b)$$

$$r_{CO} = (r_1 + r_2 - r_3) \times \frac{W_{cat}}{V_{cat}} \times M_{CO} \qquad (19c)$$

$$r_{H_2O} = -(r_2 + r_3) \times \frac{W_{cat}}{V_{cat}} \times M_{H_2O} \qquad (19d)$$

$$r_{CO_2} = r_3 \times \frac{W_{cat}}{V_{cat}} \times M_{CO_2} \qquad (19e)$$

$$r_{H_2} = (r_1 + 3r_2 + r_3) \times \frac{W_{cat}}{V_{cat}} \times M_{H_2} \qquad (19f)$$

$$q_{\mathrm{C}} = (-r_1 \Delta H_1 - r_2 \Delta H_2 - r_3 \Delta H_3) \times \frac{W_{cat}}{V_{cat}} \qquad (19g)$$

where W_{cat} and V_{cat} are the total catalyst loading (in gram) and the volume of catalyst bed, respectively.

Boundary Conditions

Inlet (z =0): $u = u_{in},\ T = T_{in},\ \dot{n}_{H_2O,in} = \psi \dot{n}_{C_2H_5OH,in}$ (20)

Exit ($z = L$): $\frac{\partial \vec{V}}{\partial z} = \frac{\partial T}{\partial z} = \frac{\partial m_i}{\partial z} = 0,\ P = P_{out}$ (21)

Along centerline (r = 0): $\frac{\partial \vec{V}}{\partial r} = \frac{\partial T}{\partial r} = \frac{\partial m_i}{\partial r} = 0$ (22)

At wall ($r = R$): $\vec{V} = 0,\ T = T_w,\ \frac{\partial m_i}{\partial r} = 0$ (23)

where u_{in}, T_{in}, $\dot{n}_{H_2O,in}, \dot{n}_{C_2H_5OH,in}$, and ψ are the velocity, temperature, molar flow rate of steam and ethanol, and the molar ratio of steam to ethanol at inlet, respectively. The fully-developed boundary conditions are specified at exit. The symmetric conditions are specified along the reactor centerline. No-slip boundary condition for the flow and no species deposition are specified at the reactor wall.

The gas hourly space velocity (GHSV) is an important parameter for a catalytic reaction process, and it is defined as,

$$\text{GHSV}\ (h^{-1}) = \dot{V}_{gas}/V_{cat} \qquad (24)$$

where $\dot{V}_{gas}$ is the inlet volumetric flow rate measured under the standard condition.

Numerical Method

The COMSOL multiphysics (Comsol Inc., version 5.1) is used to solve the governing equations and boundary conditions. The accuracy of numerical solution is related to the mesh size. Therefore, the solution independence of the mesh size was carefully studied first. The numerical results show that the solutions become mesh-independent when the element number exceeds approximately 8,000 with a maximum relative variation ≦ 10^{-4}. For the results presented in this work, 10,950 meshes were used to ensure numerical convergence and solution accuracy.

The values to evaluate the performance for ethanol steam reforming are ethanol conversion, water conversion and hydrogen selectivity defined as

$$X_{C_2H_5OH}(\%) = \frac{\dot{n}_{EtOH,in} - \dot{n}_{EtOH,out}}{\dot{n}_{EtOH,in}} \times 100\% \qquad (25)$$

$$X_{H_2O}(\%) = \frac{\dot{n}_{H_2O,in} - \dot{n}_{H_2O,out}}{\dot{n}_{H_2O,in}} \times 100\% \qquad (26)$$

where $\dot{n}_{EtOH,in}$ and $\dot{n}_{H_2O,in}$ are the molar flow rates of ethanol and water at inlet, $\dot{n}_{EtOH,out}$ and $\dot{n}_{H_2O,out}$ are the molar flow rates of ethanol and water at outlet, respectively.

RESULTS AND DISCUSSION

To verify the accuracy of numerical model, the parameters used in the experiment by Wu et al. (2014) are adopted, where the reactor length L = 21 cm, the tube radius R = 1.65 cm, the inlet steam/ethanol molar ratio ψ = 10, T_w = T_{in} = 873K, Ni/Al_2O_3 catalyst loading of 20g, and the porosity of catalyst bed ε = 0.649 are used. The comparisons of the mole fraction for each species and the conversion of the ethanol and water for varied space time τ are shown in Fig. 2 and 3, respectively. Wu et al. (2014) defined the space time (unit: second) as $\tau = V_{cat}/\dot{V}_{gas}$, which is a reciprocal of GHSV in Eq. (25). The values of τ = 1, 2, 3, and 4 seconds are corresponding to the values of GHSV at 3600, 1800, 1200, and 900 h^{-1}, respectively. According to Figs. 2 and 3, the results of numerical simulation here are consistent with the experimental data (Wu et al., 2014).

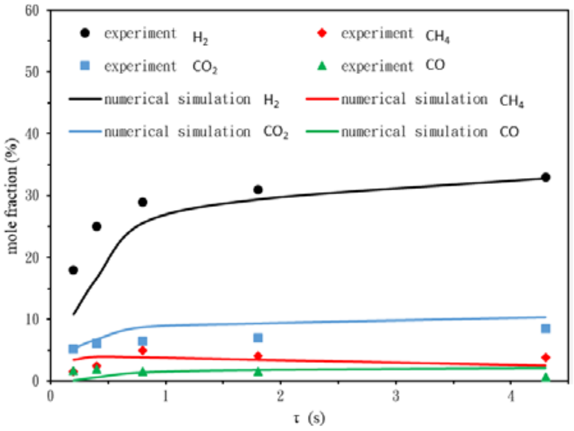

Fig. 2. Comparison of mole fraction for each species between experimental data (Wu et al., 2014) and numerical simulation for varied τ at 873K.

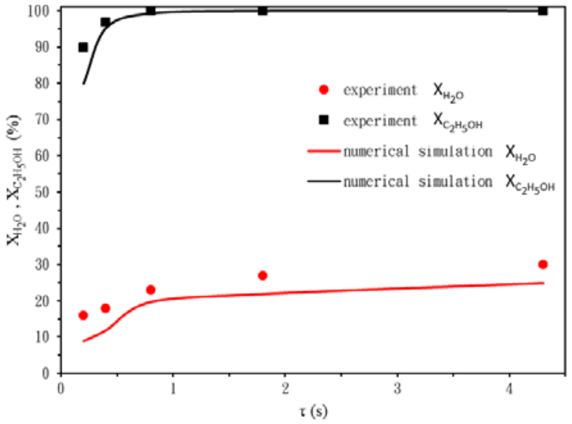

Fig. 3. Comparison of reactant conversion between experimental data (Wu et al., 2014) and numerical simulation for varied τ at 873K.

From a viewpoint of chemical kinetics given by Eqs. (9)–(11), the reaction rate of ethanol decomposition is improved as the temperature increases. One mole hydrogen is produced by the decomposition of one mole of ethanol (Eq. 9). Compared with the reaction of ethanol decomposition, the reaction of methane steam reforming is more efficient to generate hydrogen because three moles of hydrogen gas are generated by the consumption of one mole of methane (Eq. 10). The forward reaction of methane steam reforming is more active with increasing temperature. However, the backward reaction of water gas shift is enhanced at high temperature (Eq. 11). This fact implies that more CO is produced for high temperature. When the reformed syngas is supplied as fuel for the low temperature type of PEM fuel cell, both a high H_2 concentration and a very low CO concentration (< 10 ppm) are desired. The lower CO concentration in the reformed syngas is favorable for the follow-up CO reduction processes.

The distributions of species molar concentrations along the centerline (r =0) at GHSV = 2000 h^{-1} and ψ = 10 with $T_w = T_{in}$ are shown in Fig. 4(a) and 4(b) for T_w = 673 K and T_w = 873 K, respectively. The molar concentrations for each species is almost constant at exit region, that is, the reaction approaches an equlibrium state. The H_2, CH_4, and CO concentrations at exit for T_w = 673K are 5.2, 2.85 and 0.046 mol/m^3, respectively. At higher temperature of T_w = 873K, the H_2 concentration is increased to 8.18 mol/m^3, and the CH_4 concentration is decreased to 0.74 mol/m^3, but the CO concentration is remarkably increased to 0.50 mol/m^3. This is because the reactions of ethanol decomposition (Eq. 9) and methane steam reforming (Eq. 10) are endothermic, while the water gas shift reaction (Eq. 11) is exothermic. At higher temperature, the rates of endothermic reactions are enhanced such that the H_2 concentration becomes higher and the CH_4 concentration becomes lower. Conversely, the rate of reverse water gas shift reaction ($\mathrm{CO} + H_2O \rightleftharpoons CO_2 + H_2$) is more active at higher temperature, this results in a higher CO concentration at exit.

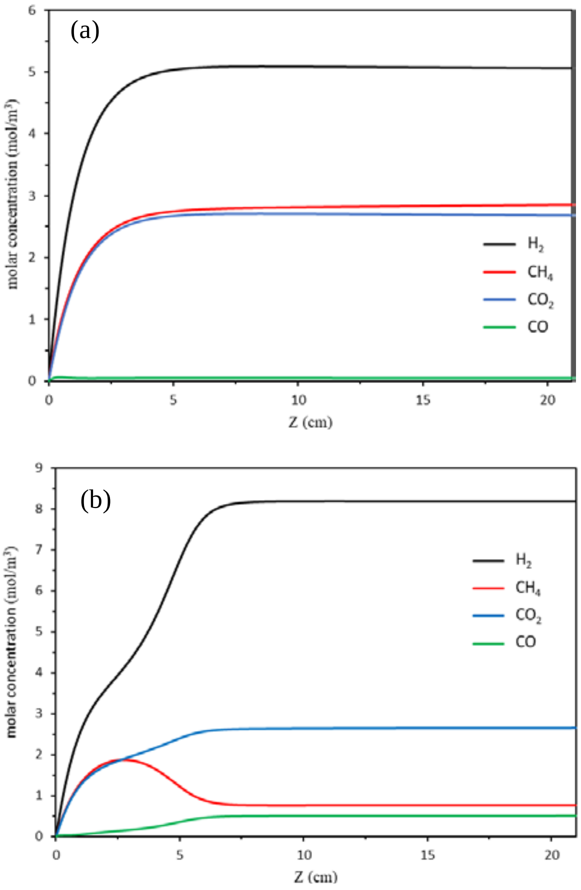

Fig. 4. The distributions of species molar concentrations along the centerline at GHSV = 2000 h^{-1} and ψ = 10 for (a) T_w = 673K, (b) T_w = 873K.

The species concentrations for T_w = 673K in Fig. 4(a) are rapidly increased at entrance region and change very small for $z > 4$ cm. It is worthy noting that the curve of CH_4 concentration at T_w = 873K shows a different behavior, shown in Fig. 4(b). The CH_4 concentration is first increased to a maximum value of 1.87 mol/m^3 at z = 2.76 cm, then it falls quickly with the further increase of z, and it approaches to the value (0.76mol/m^3) of equlibrium state for z > 7 cm. The molar concentration of methane is higher than that at equilibrium state in the vicinity of inlet region. This behavior is not found for T_w = 673K, as shown in Fig. 4(a). This can be realized since the amount of reaction heat for methane steam reforming (205.9 kJ/mol) is much higher than that for ethanol decomposition (49 kJ/mol). At higher temperature of T_w = 873K, the production rate of methane from ethanol decomposition reaction is significantly higher than the consumption rate of methane by methane steam reforming reaction in very earlier entrance region for z < 2 cm. This is due to a limited energy transferred from the high-temperature wall to the reactor where an intensely exothermic reaction of methane steam reforming occurs. Thus the CH_4 concentration is rapidly increased. When the the CH_4 concentration become higher, the methane steam reforming reaction is enhanced, and then the CH_4 concentration is decreased with the increase of z for z > 2.76 cm.

The results of ethanol conversion and water conversion versus temperature with $T_w = T_{in}$ are given by Fig. 5. The conversion of ethanol is near 100% in the temperature range of 673 K to 873 K. The reaction of ethanol decomposition is almost complete. This is due to lower reaction heat for the ethanol decomposition (49 kJ/mol). The conversion of steam increases with increasing temperature. The steam conversion is 16% at temperature of 673 K and it is increased to 23% at 873 K. This is because the consumption of steam is needed for the reaction of methane steam reforming. The rate of endothermic reaction of methane steam reforming is enhanced at higher temperature.

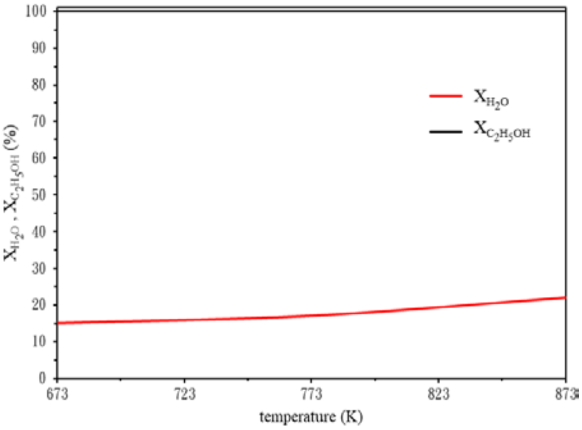

Fig. 5. The effect of temperature on ethanol conversion and water conversion for GHSV = 2000 h^{-1} and ψ = 10.

The H_2 molar concentrations at the centerline (r = 0) versus the axial coordinate (z) for varied GHSV at T_w = 873 K, ψ = 10 and T_{in} = 573 K are provided in Fig. 6. A larger value of WHSV implied that the residence time of flow in the catalyst bed becomes shorter, and chemical reaction time becomes shorter. According to Fig. 6, the molar concentrations of H_2 at exit are nearly equal to the equilibrium value of H_2 as the magnitude of GHSV is smaller than a critical value of 5000 h^{-1}. Physically, this critical value of GHSV decreases with decreasing temperature for a given reactor. With the length of reactor given here, the residence time is not enough to reach an equilibrium state at outlet for GHSV > 5000 h^{-1}.

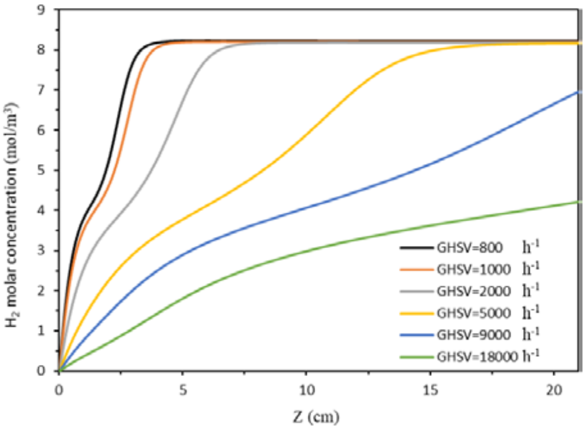

Fig. 6. The effect of GHSV on the molar concentration of H_2 for T_w = 873K, ψ = 10 and T_{in} = 573 K.

The effect of GHSV on ethanol conversion and water conversion for T_w = 873K is shown in Fig. 7. According to this figure, the ethanol conversion is approximately equal to 100% for GHSV < 4000 h^{-1}. This fact implies that the ethanol is almost consumed completely for a small magnitude of GHSV due to an enough residence time of reactants inside the reactor. Both the ethanol conversion and water conversion decrease with increasing GHSV.

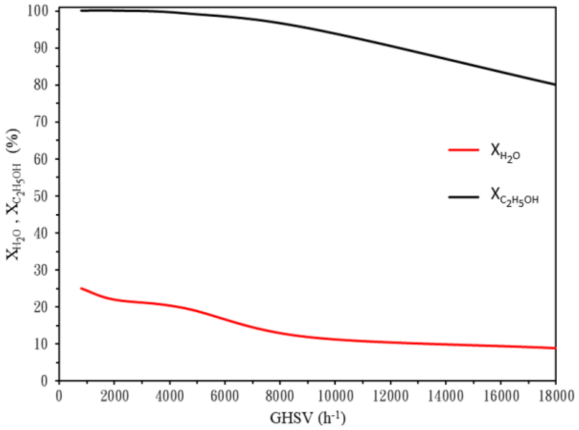

Fig. 7. The variations of the ethanol conversion and water conversion with the GHSV for T_w = 873K, ψ = 10 and T_{in} = 573 K.

As compared with other methods to produce hydrogen, the main advantage for hydrogen production by steam reforming is the higher hydrogen yield. In the steam reforming, the produced hydrogen is not only from the fuel, but it also comes from the steam. Thus it is interesting to investigate the ratio of hydrogen generated from steam. According to the overall reaction of ethanol steam reforming ($C_2H_5OH + 3H_2O \rightarrow 6H_2 + 2CO_2$), three moles of H_2 in the total 6 moles of H_2 production comes from the steam and three moles of H_2 is produced by ethanol. Consequently, a half of H_2 coming from steam and a half of H_2 coming from ethanol are theoretically obtained if a completely forward reaction of ethanol steam reforming is considered. In fact, it is expected that an equilibrium state is achieved when the residence time is long enough.

The variations of the ratios for hydrogen generated from steam and ethanol versus T_w at GHSV = 2000 h^{-1} for ψ = 3 and ψ = 10 are provided in Fig. 8(a) and 8(b), respectively. When the steam and ethanol molar ratio at inlet is stoichiometric (ψ = 3), it is shown that a high ratio (78.2%) of H_2 comes from the steam in Fig. 8(a), while only 21.8% of H_2 comes from the ethanol at T_w = 673 K. The ratio of H_2 coming from the steam is remarkably decreased with an increase in T_w, and it is overtaken by the ratio of H_2 coming from the ethanol for T_w > 852 K. At a high temperature of T_w = 873 K, the ratio of H_2 coming from steam is reduced to 48.4%, while the ratio of H_2 coming from the ethanol is significantly increased to 51.6%, which is 2.3 times of that at T_w = 673 K. The above result indicates that more than 50% of hydrogen comes from steam for T_w < 852 K. As stated above, the reaction rate of methane steam reforming (Eq. 10) increases as T_w increases. This fact implies that the ratio of H_2 generated from ethanol is increased with increasing T_w.

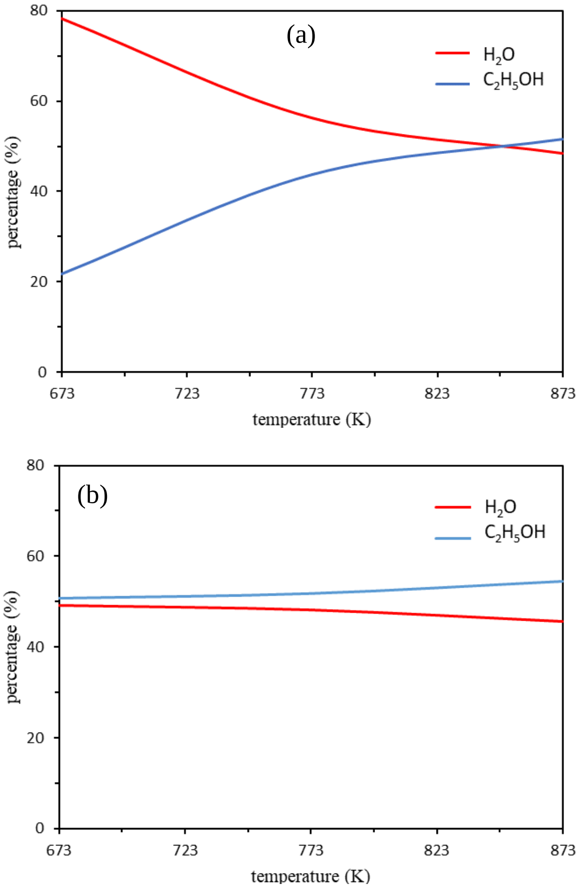

Fig. 8. The variations of the ratios for hydrogen generated from steam and ethanol versus T_w at GHSV = 2000 h^{-1} and T_{in} = 573 K for (a) ψ = 3, (b) ψ = 10.

For a higher steam/ethanol molar ratio (ψ = 10), the steam is abundant and this is beneficial for the ethanol reforming, this can be realized from the overall ethanol reaction ($C_2H_5OH+3H_2O \rightarrow 6H_2+2CO_2$) based on the Le Chatelier's principle. As shown in Fig. 8(b), the ratio of H_2 coming from the ethanol is always slightly higher than that of H_2 coming from the steam. This behavior is different from the case for T_w = 873 K. The ratio of H_2 coming from the ethanol is increased slightly with the increasing T_w. The ratio of H_2 coming from the ethanol is 50.8% at T_w = 673 K, and it becomes to 54.4% at T_w = 873 K. The ratio of H_2 coming from the steam is 49.2% at T_w = 673 K, and it becomes to 45.6% at T_w = 873 K. The above results show that the more than 45% of produced hydrogen comes from the steam in the operation conditions used in this work. This indicates that a great proportion of hydrogen coming from the steam in the ethanol steam reforming is still found even for ψ = 10.

CONCLUSIONS

The performance of ethanol steam reforming in a tubular fixed-bed reactor is investigated by a verified numerical method. Based on the parameters used in this work, the conclusions are as follows.

(1) At the inlet steam/ethanol molar ratio ψ = 10 and GHSV = 2000 h^{-1}, the concentration of methane in the vicinity of inlet region for a higher T_w of 873 K is greater than that at equilibrium state at outlet. However, this phenomenon is not observed for T_w = 673 K. The physical reason is that the reaction rate of ethanol decomposition is remarkbly higher than that of methane steam reforming around the inlet region. The H_2 concentration increases with T_w, while the CO concentration is remarkably increased from 0.046 to 0.50 mol/m^3 when T_w increases from 673 K to 873 K.

(2) The conversion of ethanol is near 100% in the temperature range of 673 K to 873 K for ψ = 10. The conversion of steam increases with the increase of T_w because the consumption of steam occurs simultaneously for the reaction of methane steam reforming.

(3) Both the ethanol conversion and water conversion are decreased with increasing GHSV because the residence time inside the reactor becomes shorter with increasing GHSV.

(4) At stoichiometric condition (ψ = 3), a high ratio (78.2%) of hydrogen comes from the steam, while only 21.8% of H_2 comes from the ethanol at T_w = 673 K. The ratio of H_2 coming from the steam is remarkably decreased with the increase of T_w, and it is overtaken by the ratio of H_2 coming from the ethanol for T_w > 852 K. At T_w = 873 K, the ratio of H_2 coming from the steam is reduced to 48.4%, while the ratio of H_2 coming from the ethanol is increased to 51.6%, which is 2.4 times of that at T_w = 673 K. For ψ = 10, the ratio of H_2 coming from the ethanol is always slightly higher than that of H_2 coming from the steam. This behavior is different from the case for T_w = 873 K. The ratio of H_2 coming from the ethanol or steam changes slightly with the increasing T_w. Overall, the more than 45% of produced hydrogen comes from the steam, and the ratio of H_2 coming from steam increases with decreasing T_w and ψ.

ACKNOWLEDGMENT

This work is funded by the Ministry of Science and Technology in Taiwan under contract of MOST 109-2221-E-007-008.

REFERENCES

Akande, A., Aboudheir, A., Idem, R., and Dalai, A., "Kinetic modeling of hydrogen production by the catalytic reforming of crude ethanol over a co-precipitated Ni/Al_2O_3 catalyst in a packed bed tubular reactor," Int. J. Hydrogen Energy, Vol. 31, pp.1707-1715 (2006).

Akpan, E., Akande, A., Aboudheir, A., Ibrahim, H., and Idem, R., "Experimental, Kinetic and 2-D reactor modeling for simulation of the production of hydrogen by the catalytic reforming of concentrated crude ethanol (CRCCE) over a Ni-based commercial catalyst in a packed-bed tubular reactor," Chem. Eng. Sci., Vol. 62, pp.3112-3126 (2007).

Bird, R.B., Stewart, W.E., and Lightfoot, E.N., *Transport Phenomena*, 2nd ed., New York: John Wiley & Sons, 2002.

Chang, S.C., Yang, C.H., Feng, T.H., and Chen, C.K., "Modeling and simulation of tubular steam methane reformer," CSME J., Vol. 40, pp.499-506 (2019).

Chen, W.H. and Lin, B.J., "Effect of microwave double absorption on hydrogen generation from methanol steam reforming," Int. J. Hydrogen Energy, Vol. 35, pp.1987-1997 (2010).

Chen, W.H., Jheng, J.G., and Yu, A.B., "Hydrogen generation from a catalytic water gas shift reaction under microwave irradiation," Int. J. Hydrogen Energy, Vol.33, pp.4789-4797 (2008).

Chen, W.H. and Chen, C.Y., "Water gas shift reaction for hydrogen production and carbon dioxide capture: A review," Applied Energy, Vol. 258, 114078 (2020).

Chen, W.H. and Lu, J.J., "Hydrogen production from water gas shift reactions in association with separation using a palladium membrane tube," Int. J. Energy Res., Vol.36, pp.346-354 (2012).

Comas, J., Mariño, F., Laborde, M., and Amadeo, N., "Bio-ethanol steam reforming on Ni/Al_2O_3 catalyst," Chem. Eng. J., Vol. 98, pp.61-68 (2004).

Contreras, J.L., Salmones, J., Colın-Luna, J.A., Nuno L., Quintana, B., Cordova, I., Zeifert, B., Tapia, C., Fuentes, G.A., "Catalysts for H_2 production using the ethanol steam reforming (a review)," Int. J. Hydrogen Energy, Vol. 39, pp.18835-18853 (2014).

Cunha, A.F., Wu, Y.J., Diaz Alvarado, F.A., Santos, J.C., Vaidya, P.D., and Rodrigues, A.E., "Steam reforming of ethanol on a Ni/Al_2O_3 catalyst coupled with a hydrotalcite-like sorbent in a multilayer pattern for CO_2 uptake," Can. J. Chem. Eng., Vol. 90, pp.1514-1526 (2012).

Freni, S., Cavallaro, S., Mondello, N., Spadaro, L., and Frusteri, F., "Production of hydrogen for MC fuel cell by steam reforming of ethanol over MgO supported Ni and Co catalysts," Catal.

Comm., Vol. 4, pp.259-268 (2003).

Holladay, J.D., Hu, J., King, D.L., and Wang, Y., “An overview of hydrogen production technologies,” Catal. Today, Vol. 139, pp.244-260 (2009).

Huang, W.J., Yu, C.T., Sheu, W.J., and Chen, Y.C., “The effect of non-uniform temperature on the sorption-enhanced steam methane reforming in a tubular fixed-bed reactor,” Int. J. Hydrogen Energy, https://doi.org/10.1016/j.ijhydene.2020.07.182

Lin, Y.S., Sheu, W.J., and Chen, Y.C., “Effect of diffuser flow on the performance of water-gas shift membrane reactors,” CSME J., Vol. 4, pp.265-274 (2020).

Llera, I., Mas, V., Bergamini, M.L., Laborde, M., and Amadeo, N., “Bio-ethanol steam reforming on Ni based catalyst. Kinetic study,” Chem. Eng. Sci., Vol. 71, pp.356–366 (2012).

Ma, R., Castro-Dominguez, B., and Dixon, A.G., “CFD study of heat and mass transfer in ethanol steam reforming in a catalytic membrane reactor,” Int. J. Hydrogen Energy, Vol. 43, pp.7662-7674 (2018).

Mathure, P.V., Ganguly, S., Patwardhan, A.V., and Saha, R.K., “Steam reforming of ethanol using a commercial nickel-based catalyst,” Ind. & Eng. Chem. Res., Vol. 46, pp.8471-8479 (2007).

Mondal, T., Pant, K.K., and Dalai, A.K., “Catalytic oxidative steam reforming of bio-ethanol for hydrogen production over Rh promoted Ni/CeO_2-ZrO_2 catalyst,” Int. J. Hydrogen Energy, Vol. 40, pp.2529-2544 (2015).

Ni, M., Leung, D., and Leung, M.A., “A review on reforming bio-ethanol for hydrogen production,” Int. J. Hydrogen Energy, Vol. 32, pp.3238-3247 (2007).

Nikolaidis, P. and Poullikkas, A., “A comparative overview of hydrogen production processes,” Renew. Sust. Energy Rev., Vol. 67, pp.597-611 (2017).

Perng, S.W., Chou, H.M., and Wu, H.W., “Numerical study of plate-shape methanol steaming reformer with a convergent fuel channel,” CSME J., Vol. 40, pp.647-653 (2019).

Sun, J., Qiu, X.P., Wu, F., and Zhu, W.T., “H_2 from steam reforming of ethanol at low temperature over Ni/Y_2O_3, Ni/La_2O_3 and Ni/Al_2O_3 catalysts for fuel-cell application,” Int. J. Hydrogen Energy, Vol. 30, pp.437-445 (2005).

Wang, C.T., Wu, J.C., Garg, A., Chong, W.T., Ong, H.C., Wu, B.X., and Jang, J.H., “Effective convergent-type flow slab in proton exchange membrane fuel cells,” CSME J., Vol. 41, pp. 85- 90 (2020).

Wu, Y.J., Santos, J.C., Li, P., Yu, J.G., Cunha, A.F., and Rodrigues, A.E., “Simplified kinetic model for steam reforming of ethanol on a Ni/Al_2O_3 catalyst,” Can. J. Chem. Eng., Vol. 92, pp.116-130 (2014).

Xu, J. and Froment, G.F., “Methane steam reforming, methanation and water-gas shift: 1. Intrinsic kinetics,” AIChE J., Vol. 35, pp.88-96 (1989).

NOMENCLATURE

C_p	specific heat, J/(kg·K)
d_p	diameter of the catalyst particles, m
D	tube diameter of reactor, mm
D_{ij}	binary molecular diffusivity, m^2/s
D_i^T	thermal diffusion coefficient, kg/(m·s)
GHSV	gas hourly space velocity, h^{-1}
ΔH	enthalpy of reaction, kJ/mol
$\overleftrightarrow{I}$	identity tensor
K	permeability, m^2
k	thermal conductivity, W/(m·K)
k_i	rate coefficient of the ith reaction
L	catalyst bed length, m
m_i	mass fraction of the ith species
M_i	molecular weight of ith species, g/mol
$\dot{n}$	molar flow rate, mol/s
P	pressure, atm
q_c	heat source/sink due to chemical reaction, W/m^3
R	reactor radius, cm
R_g	gas constant, m^3·atm/(K·mol)
r_i	production rate, mol/(m^3·s)
S_U	source term in momentum equation
T	temperature, K
T_{in}	inlet temperature, K
T_w	wall temperature, K
V_{cat}	the volume of catalyst bed, m^3
$\vec{V}$	flow velocity vector, m/s
$\dot{V}$	volume flow rate, m^3/s
W_{cat}	the total catalyst weight, g
$X_{C_2H_5OH}$	ethanol conversion
X_{H_2O}	water conversion
y_i	molar fraction of the ith species

Greek symbols

ε	porosity,
μ_m	gas mixture viscosity, Pa·s
ρ	gas mixture density, kg/m^3
ψ	inlet molar ratio of steam to ethanol

在管狀固定床反應器的乙醇蒸汽重組數值分析

黃竹愉 許文震 陳炎洲

摘要

本文以數值方法分析管型固定床乙醇蒸汽重組產氫反應器的性能，探討管的壁溫(T_w)、氣體空間速度(GHSV)及進口水蒸汽/乙醇莫爾比(ψ)的效應。於GHSV = 2000 h^{-1}條件下，結果顯示在高溫壁(T_w = 873K)及ψ =10時，在進口附近的甲烷莫爾濃度大於接近平衡的出口，然而在低溫壁(T_w = 673K)情況下，此現象消失。在低溫壁(T_w = 673K)及ψ = 3的條件下，有高達78.2%的產氣氫來自水蒸汽反應物，此比例隨壁溫增高而顯著減少，在T_w < 852 K之下，有超過一半來自水蒸汽。於ψ = 10時，產氣氫來自水蒸汽便會稍小於來自乙醇,在本文探討的參數範圍，均至少45%產氣氫來自水蒸汽。